Journal of
Synchrotron Radiation

ISSN 0909-0495

Received 1 March 2009
Accepted 23 August 2009

Development of an energy-domain ^{57}Fe-Mössbauer spectrometer using synchrotron radiation and its application to ultrahigh-pressure studies with a diamond anvil cell

Takaya Mitsui,[a,b]* Naohisa Hirao,[c,b] Yasuo Ohishi,[c] Ryo Masuda,[a,b] Yumiko Nakamura,[d] Hirotoshi Enoki,[d] Kouji Sakaki[d] and Makoto Seto[a,b,e]

[a]Japan Atomic Energy Agency, 1-1-1 Kouto, Sayo-cho, Sayo-gun, Hyogo 679-5148, Japan, [b]CREST, Japan Science and Technology Agency, 4-1-8 Honcho, Kawaguchi, Saitama 332-0012, Japan, [c]Japan Synchrotron Radiation Research Institute, 1-1-1 Kouto, Sayo-cho, Sayo-gun, Hyogo 679-5198, Japan, [d]National Institute of Advanced Industrial Science and Technology, Tsukuba Central 2, 1-1-1 Umezono, Tsukuba, Ibaraki 305-8568, Japan, and [e]Research Reactor Institute, Kyoto University, Kumatori, Sennan-gun, Osaka 590-0494, Japan. E-mail: taka@spring8.or.jp

An energy-domain ^{57}Fe-Mössbauer spectrometer using synchrotron radiation (SR) with a diamond anvil cell (DAC) has been developed for ultrahigh-pressure measurements. The main optical system consists of a single-line pure nuclear Bragg reflection from an oscillating $^{57}FeBO_3$ single crystal near the Néel temperature and an X-ray focusing device. The developed spectrometer can filter the Doppler-shifted single-line ^{57}Fe-Mössbauer radiation with a narrow bandwidth of neV order from a broadband SR source. The focused incident X-rays make it easy to measure a small specimen in the DAC. The present paper introduces the design and performance of the SR ^{57}Fe-Mössbauer spectrometer and its demonstrative applications including the newly discovered result of a pressure-induced magnetic phase transition of polycrystalline $^{57}Fe_3BO_6$ and an unknown high-pressure phase of $Gd^{57}Fe_2$ alloy placed in a DAC under high pressures up to 302 GPa. The achievement of Mössbauer spectroscopy in the multimegabar range is of particular interest to researchers studying the nature of the Earth's core.

Keywords: nuclear Bragg scattering; nuclear resonant scattering; Mössbauer spectroscopy; diamond anvil cell; high pressure; extreme conditions; phase transition; Fe_3BO_6; $GdFe_2$.

1. Introduction

The diamond anvil cell (DAC) is well recognized as a very important device for high-pressure Mössbauer spectroscopy to investigate pressure-induced effects on the magnetic properties, charge states and the local environment of a Mössbauer isotope in materials (Jayaraman, 1983). To perform high-pressure Mössbauer spectroscopy using a DAC, we generally use a radioisotope (RI) source or synchrotron radiation (SR) source as a photon source. The SR source, in particular, has many advantages: one advantage is a small beam size, which is important for studies under ultrahigh pressure using a DAC with a small gasket-hole as a sample chamber. Furthermore, the focusing device for SR X-rays allows us to obtain easily a small beam size below 100 μm diameter. In contrast, the size of the point RI source available for conventional Mössbauer spectroscopy is 0.5 mm × 0.5 mm, much larger than the beam size of the SR X-rays.

In high-pressure SR Mössbauer spectroscopy, so-called nuclear forward scattering (NFS) is normally used to obtain the hyperfine splitting (HFS) parameters, including the hyperfine field (H_{int}), the isomer shift (IS) and the quadrupole splitting (QS). In this method, time-domain interference of the delayed nuclear resonant scattering of SR pulses is measured, and the HFS parameters are determined by numerical analysis of the quantum beats in the obtained NFS time spectrum. The frequencies of the quantum beats reflect the energy splitting of the nuclear states owing to the hyperfine interactions. Experimentally, the first high-pressure NFS spectra were measured by Nasu and co-workers (Nasu, 1994) and the measurement technique has been developed rapidly with the advent of third-generation SR sources (Lübbers *et al.*, 1999; Sturhahn & Jackson, 2007). Time-domain measurement, however, requires special bunch modes of SR, *i.e.* a rather long period ($T > 100$ ns for ^{57}Fe nuclei) between electron bunches in a storage ring; such bunch operation modes are usually

limited at SPring-8, the third-generation synchrotron radiation facility in Japan. Currently, the available machine time for high-pressure SR ^{57}Fe-Mössbauer spectroscopy with NFS might be a few weeks per year at SPring-8. Moreover, NFS measurements with short bunch period may make it difficult to analyze the spectrum consisting of complex and/or multi-site hyperfine interactions particularly for users of conventional Mössbauer spectroscopy. Such situations contrast with conventional Mössbauer spectroscopy, which has a long history concerning the data analysis of the energy domain absorption spectrum measured with RI sources.

We have recently developed a new high-pressure SR ^{57}Fe-Mössbauer spectrometer using a pure nuclear Bragg reflection from an oscillating $^{57}FeBO_3$ single crystal near the Néel temperature, which can filter 14.4 keV single-line ^{57}Fe-Mössbauer radiation from broadband SR (Chumakov *et al.*, 1990; Smirnov *et al.*, 1997; Smirnov, 2000; Mitsui *et al.*, 2007*a*,*b*,*c*). As a result, it allows researchers to perform SR-based energy-domain Mössbauer spectroscopy under any bunch-mode operation of SR. Furthermore, the high degree of polarization, full recoillessness, extremely small divergence, small beam size and other excellent beam properties of SR offer the new possibility of various advanced measurement techniques fusing conventional Mössbauer spectroscopy with modern high-precision X-ray optics (Pankhurst *et al.*, 2001; Mitsui *et al.*, 2007*d*, 2008; Masuda *et al.*, 2008). In the present paper we describe the principle and component devices of the developed spectrometer. As application studies, we present two experimental results concerning high-pressure Mössbauer studies of an iron orthoborate $^{57}Fe_3BO_6$ and an intermetallic compound $Gd^{57}Fe_2$.

2. Principle of SR ^{57}Fe-Mössbauer spectroscopy with nuclear monochromator

Fig. 1 shows schematically the principle of energy-domain SR ^{57}Fe-Mössbauer spectroscopy with a variable-frequency nuclear monochromator (VFNM) (Mitsui *et al.*, 2007*c*). In this method, an electronically forbidden pure nuclear Bragg reflection from a $^{57}FeBO_3$ single crystal near the Néel temperature achieves an extremely high suppression of electronic Thomson scattering and filters 14.4 keV single-line ^{57}Fe-Mössbauer radiation from a SR source. Here, a purely nuclear Bragg reflection is allowed for the (*hkl*) lattice plane of $^{57}FeBO_3$ with the conditions $h + k + l$ = odd. The extremely narrow energy bandwidth of neV order is realised by the collapse of the nuclear Bragg reflection near the Néel temperature in the presence of a small magnetic field, $H_{ex} \simeq$ 100 Oe (Smirnov *et al.*, 1986).

As shown in Fig. 1(*a*), the SR ^{57}Fe-Mössbauer radiation is emitted at a fixed beam position by the moving crystal parallel to the reflection plane. Then, the nuclear resonance energy is shifted by the Doppler effect of light according to

$$E_{\rm ref} = E_0\left[1 + (v/c)\cos\theta_{\rm B}\right]. \qquad (1).$$

Here, E_0 is the nuclear resonance energy of ^{57}Fe nuclides in the crystal at rest, v is the velocity of the crystal, c is the velocity of light, $\theta_{\rm B}$ is the Bragg angle and $E_{\rm ref}$ is the energy of the reflected SR ^{57}Fe-Mössbauer radiation in the laboratory system. In this system, if a sample is placed at position A or B in Fig. 1(*a*), the Mössbauer spectrum in both cases can be measured equally by counting the reflected SR ^{57}Fe-Mössbauer radiation as a function of velocity, as shown in Fig. 1(*b*). Here, in the case of the former position (A), the VFNM functions as a nuclear energy analyzer.

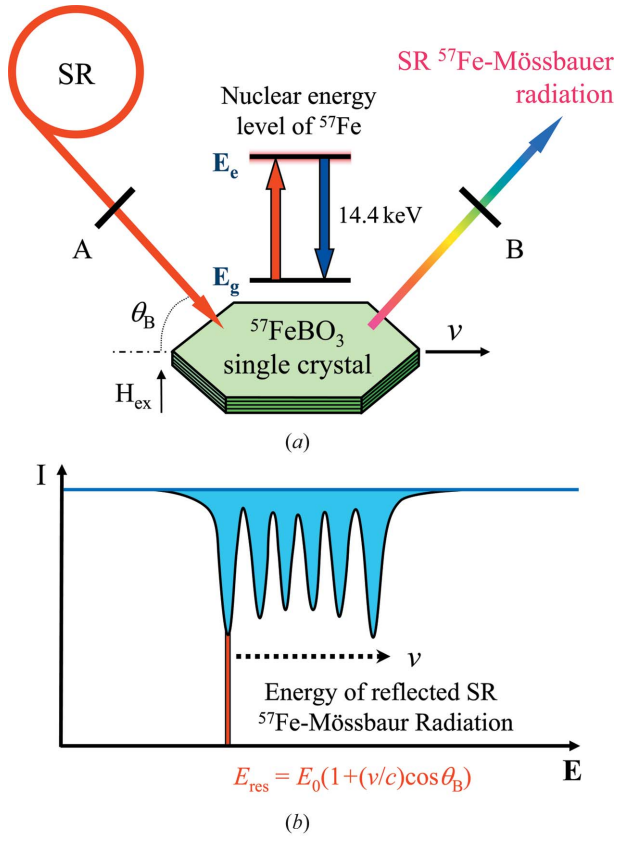

Figure 1
Conceptual diagram of energy-domain SR ^{57}Fe-Mössbauer spectroscopy with a VFNM. (*a*) Basic principle of the VFNM. (*b*) Scheme of the energy scan process for obtaining the Mössbauer spectrum.

3. Nuclear monochromator system installed at BL11XU of SPring-8

To develop materials science using energy-domain SR ^{57}Fe-Mössbauer spectroscopy, a nuclear monochromator system has been designed and installed at the JAEA beamline (BL11XU) of SPring-8. The system consists of a VFNM unit and a precision diffractometer. Their external views are shown in Figs. 2(*a*) and 2(*b*), respectively.

The VFNM utilizes a large, very high quality 95%-^{57}Fe-enriched $^{57}FeBO_3$ single crystal to filter high-throughput 14.4 keV ^{57}Fe-Mössbauer radiation from SR (see Fig. 2*a*). The crystal is grown by the flux method (Mitsui *et al.*, 2005). It is formed as a thin platelet with its surface parallel to the (111) easy magnetization plane. In that work, plane-wave X-ray topography proves that there is no curvature or growth boundaries throughout the whole crystal surface beyond

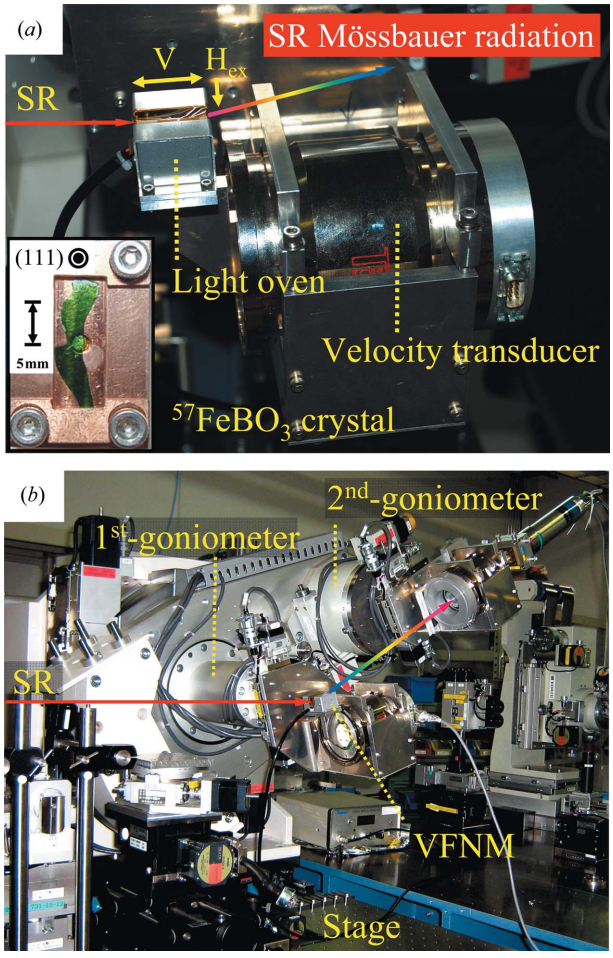

Figure 2
The nuclear monochromator system installed at BL11XU of SPring-8. (*a*) Light oven for heating an oscillating $^{57}FeBO_3$ single crystal. (*b*) External view of the high-precision diffractometer for nuclear Bragg scattering.

1.0 arcsec. In order to heat the crystal to the Néel temperature, a light oven, of weight 95 g, is used. The crystal is placed on a copper heating stage and is covered with a compact aluminium case, which is partially shielded by a Kapton polyimide film for a beam access area. The temperature of a $^{57}FeBO_3$ crystal is precisely stabilized with a precision within 0.01 K near the Néel temperature. Then, built-in small adjustable magnetic poles apply the external magnetic field within the range 100–150 Oe to the crystal surface and normal to the scattering plane. Under these conditions the heated crystal is oscillated parallel to the basal (111) plane using a Mössbauer velocity transducer (WissEL MVT-1000).

In order to perform high-resolution measurements of nuclear Bragg reflections from the $^{57}FeBO_3$ crystal, a special diffractometer has also been installed at BL11XU. As shown in Fig. 2(*b*), it consists of two high-precision goniometers and some motorized swivel and translation stages. The device parameters are summarized in Table 1.

In normal mode, the VFNM unit is attached to the first goniometer, and the Bragg angle of a $^{57}FeBO_3$ single crystal is adjusted with a high angular resolution below 1.0 arcsec. As an advantage of this apparatus, the first goniometer is equipped with a special load compensation mechanism on the 2θ axis. In future application studies, it will support the use of additional optical components and heavy experimental devices downstream of the VFNM.

Table 1
Parameters of the high-precision diffractometer of the VFNM.

	Range	Resolution	Capacity
First goniometer			
θ	$\pm 90°$	0.00002°	500 kg
2θ arm	$-45°$ to $150°$	0.0001°	250 kg
Swivel (Rx_1)	$\pm 10°$	0.000765°	5 kg
Z-axis (Z_1)	± 10 mm	0.25 mm	10 kg
Horizontal travel			
Coarse	± 100 mm	(manual)	
Fine	± 15 mm	0.16 mm	
Second goniometer			
θ	$\pm 90°$	0.0001°	25 kg
2θ arm	$\pm 90°$	0.0002°	10 kg
Swivel (Rx_2)	$\pm 10°$	0.000765°	5 kg
Z-axis (Z_2)	± 10 mm	0.25 mm	10 kg
Stage size	650 × 1150 × 1040 (−200 to +50); vertical axis, driven by stepping motor		

4. Energy-domain SR Mössbauer spectrometer for high-pressure measurement

The application of ultrahigh-pressure Mössbauer spectroscopy requires measurements on the extremely small sample enclosed in the DAC. Therefore, we have developed a new energy-domain high-pressure SR ^{57}Fe-Mössbauer spectrometer (HP-SRMS), which makes it possible to perform small-target research with a high signal-to-noise ratio. The main optical components are a high-resolution monochromator, an X-ray focusing mirror and a VFNM system. The external view and optics of the spectrometer are shown in Figs. 3(*a*) and 3(*b*), respectively.

The experimental procedure is as follows. The electron current of the SPring-8 storage ring is kept at 100 mA at 8.0 GeV by its 'top-up' operation (Tanaka *et al.*, 2006). A liquid-nitrogen-cooled Si(111) double-crystal monochromator is used to handle the high heat load of undulator radiation (Shiwaku *et al.*, 2004), and σ-polarized incident X-rays with an energy width of 2.5 meV at 14.4 keV nuclear resonance of ^{57}Fe are produced by a nested high-resolution monochromator (HRM) consisting of asymmetric Si(511) and asymmetric Si(975) channel-cut crystals (Mitsui *et al.*, 2001). The beam size is 0.4 mm × 1.8 mm and the total flux is 1.0×10^{10} counts s^{-1}, typically. A small-size probe beam is obtained using a bent elliptical multilayer X-ray focusing mirror (MXFM), which is coated with 50 layers of W(13 Å)/Si(39.5 Å) on a high-quality quartz SiO_2 base (Mitsui *et al.*, 2004). Here, the incident X-rays are reflected at a Bragg peak angle of 8.6 mrad and are horizontally focused with a size of 400 µm × 20 µm at the focus position (F) 600 mm downstream from the centre position of the MXFM. The total flux is about 4.5×10^9 counts s^{-1}. The focused X-rays are ultrafinely monochromated to a

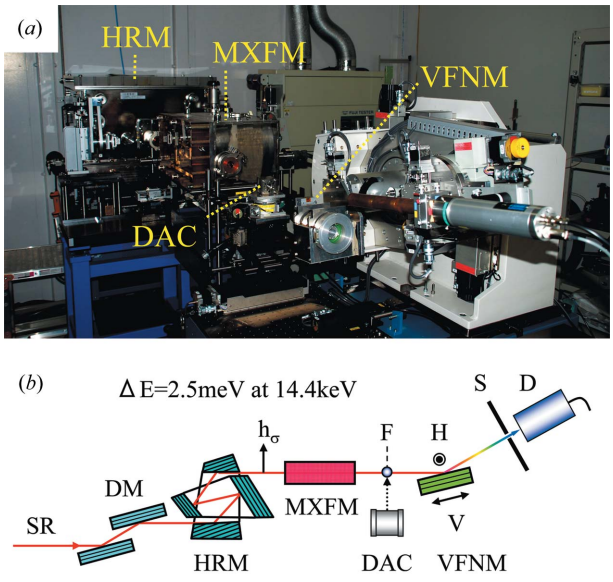

Figure 3
SR ^{57}Fe-Mössbauer spectrometer for ultrahigh-pressure measurements. (*a*) External view, (*b*) nuclear diffraction optics. SR: synchrotron radiation from the undulator of BL11XU; DM: double-crystal monochromator, Si 111 reflections; HRM: high-energy resolution monochromator, nested-type channel-cut Si 511 × Si 975 reflections; MXFM: multilayer X-ray focusing mirror; F: focusing position; VFNM: variable-frequency nuclear monochromator; $^{57}FeBO_3$ crystal near the Néel temperature; H: magnetic field; S: 0.4 mm × 5.0 mm slit; D: NaI detector.

bandwidth of about 15.4 neV by a VFNM using a single-line pure nuclear Bragg reflection from a $^{57}FeBO_3$ single crystal near the Néel temperature (348.8 K) in a 150 Oe external field. In order to change the nuclear resonance energy, the crystal is oscillated in the sinusoidal velocity mode with a frequency range of $8.0 \leq f \leq 10.0$ Hz. Behind a slit (S), the nuclear Bragg diffracted X-rays are detected by a NaI scintillation detector. The typical peak photon-counting rates of $^{57}FeBO_3$ (111) and (333) reflections are about 7.5×10^3 and 3.5×10^3 counts s^{-1}, respectively. Their noise levels are below 4.0%. In this optics, if the sample enclosed in the DAC is placed at the beam focus position (F), the Mössbauer absorption spectrum can be measured by counting the intensity of a single-line nuclear Bragg reflection as a function of velocity as described in §2.

5. Application experiments

To evaluate the experimental performance of the HP-SRMS, we have carried out high-pressure studies of polycrystalline $^{57}Fe_3BO_6$ and $Gd^{57}Fe_2$. The latter is, to our knowledge, the first report on Mössbauer spectroscopy under multimegabar pressures (up to $P \simeq 300$ GPa).

5.1. Pressure-induced phase transition from the antiferromagnetic to non-magnetic state in $^{57}Fe_3BO_6$

Under ambient pressure, iron orthoborate Fe_3BO_6 belongs to the space group D_{2h}^{16} (*Pnma*) and below $T_N = 508$ K represents an antiferromagnetic structure with weak ferromagnetism. The elemental cell contains 12 Fe^{3+} ions occupying non-equivalent 4*c* and 8*d* sites and the ^{57}Fe-Mössbauer spectrum shows a typical profile with multi-site hyperfine interactions (Wolfe *et al.*, 1969). Although there are many papers dealing with the magnetic properties of Fe_3BO_6, the high-pressure phase is still unknown. Therefore, we have carried out SR Mössbauer spectroscopy of Fe_3BO_6 under high pressure as the first performance-test experiment of the HP-SRMS.

Isotopically enriched polycrystalline samples were prepared by grinding the flux-grown $^{57}Fe_3BO_6$ (^{57}Fe, 95%) crystal in an agate mortar. The sample and small ruby chips were enclosed in a hole of diameter 59 µm in a rhenium gasket between the bevelled-diamond anvils of 150 µm culet size. NaCl was used as the pressure-transmitting medium. The pressure was estimated using the shift of the ruby R1 fluorescence line. The pressure inhomogeneity was estimated to be less than 2.0 GPa from ruby chips in the sample chamber.

SR ^{57}Fe-Mössbauer spectra in the pressure range $0 \leq P \leq 59$ GPa were measured at room temperature by a VFNM using the $^{57}FeBO_3$ (333) reflection plane. Statistically sufficient spectra were obtained with a short measurement time of 2.0 h. This shows the high potential of the HP-SRMS in high-pressure studies using a DAC. Note that typical data collection times for such high-pressure measurements using a RI source is several days or more.

Fig. 4 presents typical absorption spectra for different pressures. From the results of data fitting, one can recognize that all spectra consist of two hyperfine subspectra with an intensity ratio of 1:2. This is clear evidence that the iron atoms are in two non-equivalent crystallographic sites over the whole pressure range up to 59 GPa. The calculated HFS parameters are plotted in Fig. 5.

At ambient pressure, the spectrum shows well resolved Zeeman sextets owing to 4*c* and 8*d* iron sites. The hyperfine fields were 45.3 and 42.2 T, respectively. These values were in good agreement with previous results (Wolfe *et al.*, 1969). Here, the parameters IS and QS are typical of the Fe^{3+} high-spin (HS) $3d^5$ state ($S = 5/2$) in an octahedral environment (Wolfe *et al.*, 1969; Greenwood & Gibb, 1971).

In the pressure range $0 < P < 49$ GPa, the hyperfine fields at the 4*c* and 8*d* sites show a gradual increase up to 48.1 and 46.4 T, respectively. This is likely to be due to the increase in Néel temperature caused by the strengthening of the exchange interaction with the lattice volume decrease. In contrast, the IS and QS parameters show no pronounced pressure effect up to 49 GPa. In Fig. 5, the negative slope in IS (P) reflects only the increase in *s*-electron density at the ^{57}Fe nucleus with pressure.

At $P \geq 49$ GPa, new non-magnetic quadrupole doublets appear at the centre position of the spectrum and its abundance clearly increases with pressure. Then, all HFS parameters change abruptly at around $P = 49$ GPa as shown in Fig. 5. These results give clear evidence of the magnetic phase transition of the antiferromagnet Fe_3BO_6 state to the non-magnetic state. The coexistence of a magnetic and a non-magnetic phase is presumably due to the effect of pressure gradients. Actually, at $P = 59$ GPa, all of the iron transforms

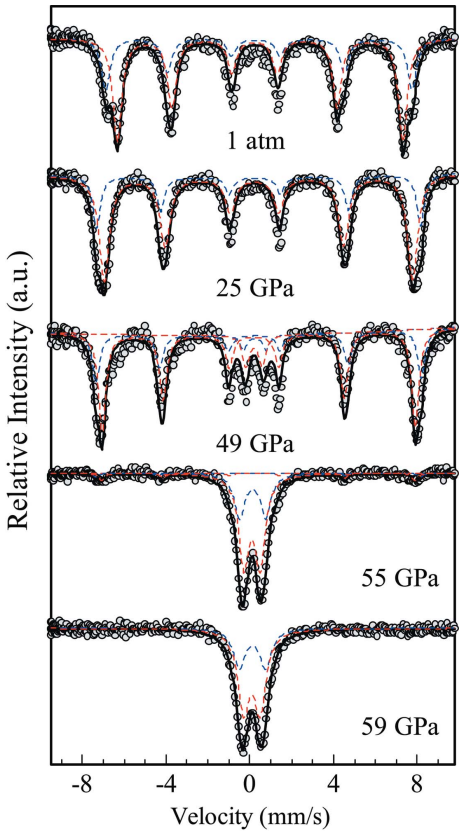

Figure 4
Room-temperature SR ^{57}Fe-Mössbauer spectra of polycrystalline $^{57}Fe_3BO_6$ for pressures below and above the magnetic phase transition. Solid and dashed lines correspond to calculations.

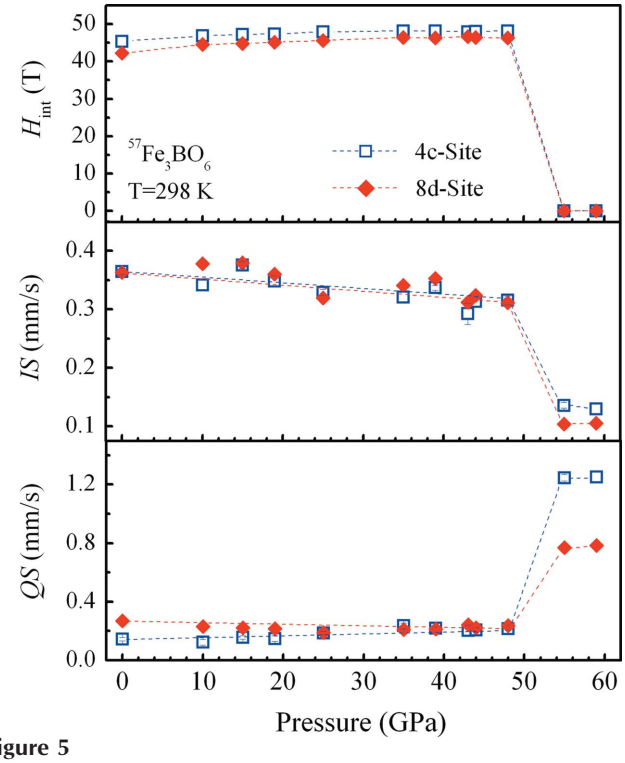

Figure 5
Experimental results for the hyperfine splitting parameters obtained from the room-temperature SR Mössbauer spectroscopy of polycrystalline $^{57}Fe_3BO_6$. Dashed lines act as guides to the eye.

into the non-magnetic phase and the spectrum shows an asymmetric doublet which consists of the two quadrupole subspectra with an intensity ratio of 1:2. Their IS are almost the same value, 0.1 mm s^{-1}, which is the typical value of the Fe^{3+} ions in the low-spin (LS) state (S = 1/2) (Greenwood & Gibb, 1971). On the other hand, the QS show different values of 1.25 mm s^{-1} and 0.79 mm s^{-1}, respectively, which implies that two different iron sites exist in $^{57}Fe_3BO_6$ after the transition. These results suggest that the pressure-induced transition of Fe_3BO_6 is strongly related to an isostructural HS $\rightarrow$ LS transition. Recently, similar phase transition behaviour has been observed in $^{57}FeBO_3$, whose magnetic moment collapses with the spin crossover HS $\rightarrow$ LS at a pressure of about 46 GPa. The change of the magnetic and electronic structures is explained by Mott's transition with rupturing of strong *d*–*d*-electron correlations (Troyan *et al.*, 2001; Sarkisyan *et al.*, 2002).

In the present preliminary study using a HP-SRMS, at least, we could observe a new pressure-induced magnetic phase transition of Fe_3BO_6, accompanying drastic changes of the electronic structure of iron. However, to elucidate the more detailed mechanism of the high-pressure-induced transition in Fe_3BO_6, we require additional measurements involving Mössbauer spectroscopy at low temperature, X-ray diffraction and electric conductivity in a DAC.

5.2. High-pressure SR Mössbauer spectroscopy of $GdFe_2$ in the multimegabar range

The intermetallic compound $GdFe_2$ under ambient conditions is a ferrimagnet with high T_c ($\sim$790 K) and belongs to the cubic C15 Laves phase structure with space group $Fd\bar{3}m$. Although the structural and magnetic properties are generally well understood, there are few reports on its high-pressure study. Nevertheless, one can expect that the magnetism of $GdFe_2$ exhibits some unusual behaviour in the high-pressure phase. This is because the magnetism in $GdFe_2$ arises not only from the itinerant 3*d* electrons of Fe atoms but also from the localized 4*f* electrons of Gd atoms; the former is strongly influenced by pressure compared with the latter. As a typical phenomenon, the high-pressure studies using NFS demonstrate that the magnetic order of $GdFe_2$ is maintained in the whole pressure region up to 105 GPa (Lübbers *et al.*, 1999). In addition, it has also been suggested that a pressure-induced (C15 $\rightarrow$ C14) structural phase transition of $GdFe_2$ occurs in the high-pressure phase above 50 GPa (Lübbers *et al.*, 1999; Reiß, 2000). To understand such phenomena in detail, it is essentially important to perform a high-pressure study of $GdFe_2$ in the multimegabar range. Therefore, as a feasibility study in the multimegabar pressure range with HP-SRMS, we have carried out SR ^{57}Fe-Mössbauer spectroscopy of $GdFe_2$ under high pressures up to 302 GPa.

A ^{57}Fe-95%-enriched $Gd^{57}Fe_2$ alloy was prepared by arc melting in an argon atmosphere. In order to obtain a single phase of $GdFe_2$, the ingot was annealed at 1073 K for 200 h in a vacuum chamber. Polycrystalline samples were obtained by grinding the ingot sample in an agate mortar. A symmetrical

diamond anvil cell with double-bevelled diamond anvils with 30 μm culet was used to generate multimegabar pressures. The sample was loaded into a hole of diameter 18 μm in a rhenium gasket without a pressure medium. The pressure gradients in the sample chamber were estimated to be less than 10 GPa at a maximum pressure of 302 GPa. Normally, we use the equations of state of elemental metals (*e.g.* Pt, Au *etc.*) for determination of the sample pressure in the multimegabar pressure range. Consequently, synchrotron radiation X-ray diffraction (SR-XRD) experiments are required for measuring the volume compression data of them. However, in the present experiment we could not carry out SR-XRD and SR-Mössbauer spectroscopy during the same SR machine time. Therefore, a diamond anvil Raman gauge was used as a practical pressure-determination method in the multimegabar pressure range without using SR-XRD (Akahama & Kawamura, 2004, 2007). The room-temperature SR ^{57}Fe-Mössbauer spectra of $Gd^{57}Fe_2$ under high pressures up to 302 GPa were measured by a VFNM using the $^{57}FeBO_3$ (111) reflection plane.

Fig. 6 presents the Mössbauer spectra of $Gd^{57}Fe_2$ for different pressures. Each spectrum has been measured with a considerably short data collection time of 3.0 h. In spite of the ultrahigh-pressure measurements up to 302 GPa, all spectra are obtained with good statistical quality. These results prove that the HP-SRMS easily realises even ultrahigh-pressure SR ^{57}Fe-Mössbauer spectroscopy in the multimegabar region. One should note that such measurements have not been achieved by conventional RI-Mössbauer spectroscopy.

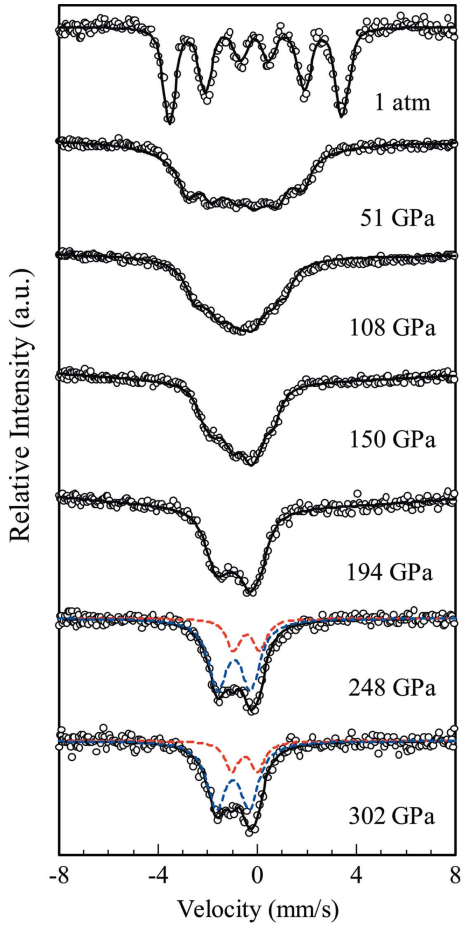

Figure 6
Room-temperature SR ^{57}Fe-Mössbauer spectra of polycrystalline $Gd^{57}Fe_2$ under multimegabar pressures. Solid and dashed lines correspond to calculations.

At ambient pressure the spectrum is fitted by a superposition of four Zeeman sextets, which agrees with the well known model of a random orientation of magnetic easy axis relative to the crystallographic directions. The estimated HFS values are consistent with previous studies (Atzmony & Dariel, 1974; Genin *et al.*, 1981; Mori *et al.*, 1998).

When the pressure rises to 51 GPa, the splitting of resonance lines decreases because of a decrease in the hyperfine field at the iron nuclei. Moreover, at a glance, one can observe an additional broadened absorption dip at the centre portion of the spectrum. The new subspectral component indicates a principle change of structural and magnetic properties of $GdFe_2$. In the pressure range $51 < P \leq 302$ GPa, the hyperfine field decreases gradually with the build up of pressure and finally disappears at about 194 GPa. The strong magnetic conservation in a high-pressure phase originates in the effect of the localized 4*f* electrons of Gd (Lübbers *et al.*, 1999). On the other hand, at $P \geq 248$ GPa, the spectra of non-magnetic $GdFe_2$ clearly show the two well resolved quadrupole doublets, corresponding to the two crystallographically non-equivalent iron sites. The intensity ratio of the corresponding lines of two components is approximately in the ratio 3:1 (see the calculated dashed lines in Fig. 6). This result strongly suggests that the high-pressure phase of $GdFe_2$ is a hexagonal C14 structure, which is likely formed by a pressure-induced structural phase transition at about 50 GPa. This is because, in the non-magnetic C14 structure, the iron atoms are generally located on the two crystallographically non-equivalent sites (6*h* and 2*a*) with an abundance ratio of 3:1. In contrast, $GdFe_2$ is in the C15 structure; all the iron sites are located in equivalent sites in the absence of a hyperfine magnetic field (Atzmony & Dariel, 1974). Therefore, the nuclear quadrupole interaction is axially symmetric, and only the doublet of one component should be observed. However, this is contradictory to the present experimental results. Actually, the spectra above 51 GPa have been fitted well by assuming $GdFe_2$ in the C14 structure. The calculated results for the averaged hyperfine structure parameters (H_{avg}, IS_{avg} and QS_{avg}) are plotted in Fig. 7. As was expected, at $P = 51$ GPa, IS_{avg} and QS_{avg} show significant changes compared with the corresponding values at ambient pressure. In contrast, at pressures above 51 GPa they show no pronounced pressure dependence up to 302 GPa. These results also provide clear evidence of the pressure-induced structural transition of $GdFe_2$ from the C15 to the C14 phase at about 50 GPa (Lübbers *et al.*, 1999). However, the details of the mechanism are not explained completely. Currently, in order to elucidate the structural and magnetic properties on the high-pressure phase in $GdFe_2$ in more detail, we are preparing further high-pressure measurements in the multimegabar range, including SR-XRD and SR-Mössbauer spectroscopy at low temperature.

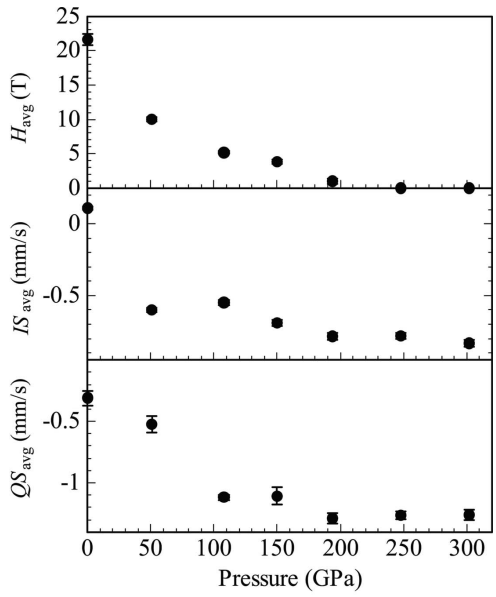

Figure 7
Experimental results for the averaged hyperfine splitting parameters obtained from the room-temperature SR ^{57}Fe-Mössbauer spectroscopy of polycrystalline $Gd^{57}Fe_2$.

6. Conclusion

A new SR-based ^{57}Fe-Mössbauer spectrometer, consisting of a HRM, a MXFM and a VFNM, has been developed for performing high-pressure studies. It allows us to perform energy-domain high-pressure SR ^{57}Fe-Mössbauer spectroscopy using a DAC of micrometre-scale gasket-hole size.

In application studies, this spectrometer could observe clearly a pressure-induced magnetic phase transition of $^{57}Fe_3BO_6$ at about 50 GPa and a new high-pressure phase of non-magnetic $Gd^{57}Fe_2$ with C14 hexagonal structure in the multimegabar region. In particular, the latter study demonstrates that the spectrometer can probe different solid-state properties at multimegabar pressures. It promises that the spectrometer can become a powerful tool for the research field of the interior of the Earth and planets in future studies; this is because the pressure in the iron-alloy core of the Earth ranges from 135 GPa to 365 GPa.

The authors would like to thank Professor S. Kikuta, Professor S. Nasu and Dr K. Aoki for various fruitful discussions, valuable comments and continuous encouragement, respectively. The authors are also grateful to the accelerator groups of SPring-8 for the excellent top-up operation. This work was partly supported by the New Energy and Industrial Technology Development Organization (NEDO) under the Advanced Fundamental Research Project on Hydrogen Storage Materials. NH was partially supported by a Grant-in-Aid for Scientific Research from the Ministry of Education, Culture, Science, Sport and Technology of the Japanese Government.

References

Akahama, Y. & Kawamura, H. (2004). *J. Appl. Phys.* **96**, 3748–3751.
Akahama, Y. & Kawamura, H. (2007). *High Press. Res.* **27**, 473–482.
Atzmony, U. & Dariel, M. P. (1974). *Phys. Rev. B*, **10**, 2060–2067.
Chumakov, A. I., Zelepukhin, M. V., Smirnov, G. V., Van Bürck, U., Rüffer, R., Hollatz, R., Rüter, H. D. & Gerdau, E. (1990). *Phys. Rev. B*, **41**, 9545–9547.
Genin, J. M., Bauer, Ph. & Besnus, M. J. (1981). *Phys. Status Solidi A*, **64**, 325–333.
Greenwood, N. N. & Gibb, T. C. (1971). *Mössbauer Spectroscopy*, p. 91. London: Chapman and Hall.
Jayaraman, A. (1983). *Rev. Mod. Phys.* **55**, 65–108.
Lübbers, R., Wortmann, G. & Grünsteudel, H. (1999). *Hyperfine Interact.* **123/124**, 529–559.
Masuda, R., Mitsui, T., Kitao, S., Higashitaniguchi, S., Yoda, Y. & Seto, M. (2008). *Jpn. J. Appl. Phys.* **47**, 8087–8090.
Mitsui, T., Kitao, S., Zhang, X. W., Marushita, M. & Seto, M. (2001). *Nucl. Instrum. Methods Phys. Res. A*, **467–468**, 1105–1108.
Mitsui, T., Kobayashi, Y. & Seto, M. (2004). *Jpn. J. Appl. Phys.* **43**, 389–393.
Mitsui, T., Seto, M., Hirao, N., Ohishi, Y., Kobayashi, Y., Higashitaniguchi, S. & Masuda, R. (2007*d*). *Jpn. J. Appl. Phys.* **46**, L382–L384.
Mitsui, T., Seto, M., Kikuta, S., Hirao, N., Ohishi, Y., Takei, H., Kobayashi, Y., Kitao, S., Higashitaniguchi, S. & Masuda, R. (2007*a*). *Jpn. J. Appl. Phys.* **46**, 821–825.
Mitsui, T., Seto, M. & Masuda, R. (2007*c*). *Jpn. J. Appl. Phys.* **46**, L930–L932.
Mitsui, T., Seto, M., Masuda, R., Kiriyama, K. & Kobayashi, Y. (2007*b*). *Jpn. J. Appl. Phys.* **46**, L703–L705.
Mitsui, T., Seto, M., Masuda, R., Kobayashi, Y. & Kitao, S. (2008). *Jpn. J. Appl. Phys.* **47**, 7136–7139.
Mitsui, T., Takei, H., Kitao, S., Seto, M., Harami, T., Zhang, X. W., Yoda, Y. & Kikuta, S. (2005). *Trans. Mater. Res. Soc. Jpn*, **30**, 7–10.
Mori, K., Onodera, H., Aoki, K. & Masumoto, T. (1998). *J. Alloys Compd.* **270**, 35–41.
Nasu, S. (1994). *Hyperfine Interact.* **90**, 59–75.
Pankhurst, Q. A., Cohen, N. S., Barquín, L. F., Gibbs, M. R. J. & Smirnov, G. V. (2001). *J. Non-Cryst. Solids*, **287**, 81–87.
Reiß, G. (2000). Dissertation, Paderborn University, Germany (downloadable from http://deposit.ddb.de/cgi-bin/dokserv?idn=961546808&dok_var=d1&dok_ext=pdf&filename=961546808.pdf).
Sarkisyan, V. A., Troyan, I. A., Lyubutin, I. S. Gavrilyuk, A. G. & Kashuba, A. F. (2002). *JETP Lett.* **76**, 788–793.
Shiwaku, H., Mitsui, T., Tozawa, K., Kiriyama, K., Harami, T. & Mochizuki, T. (2004). *AIP Conf. Proc.* **705**, 659–662.
Smirnov, G. V. (2000). *Hyperfine Interact.* **125**, 91–112.
Smirnov, G. V., van Bürck, U., Chumakov, A. I., Baron, A. Q. R. & Rüffer, R. (1997). *Phys. Rev. B*, **55**, 5811–5815.
Smirnov, G. V., Zelepukhin, M. V. & Van Bürck, U. (1986). *JETP Lett.* **43**, 352–355.
Sturhahn, W. & Jackson, J. M. (2007). *Geol. Soc. Am. Spec. Pap.* **421**, 157–174.
Tanaka, H. *et al.* (2006). *J. Synchrotron Rad.* **13**, 378–391.
Troyan, I. A., Gavrilyuk, A. G., Sarkisyan, V. A., Lyubutin, I. S., Rüffer, R., Leupold, O., Barla, A., Doyle, B. & Chumakov, A. I. (2001). *JETP Lett.* **74**, 26–29.
Wolfe, R., Pierce, R. D., Eibschütz, M. & Nielsen, J. W. (1969). *Solid. State Commun.* **7**, 949–952.